Optical Engineering

SPIEDigitalLibrary.org/oe

Design of fiber coupled Er^{3+}: chalcogenide microsphere amplifier via particle swarm optimization algorithm

Giuseppe Palma
Pietro Bia
Luciano Mescia
Tetsuji Yano
Virginie Nazabal
Jun Taguchi
Alain Moréac
Francesco Prudenzano

Design of fiber coupled Er^{3+}:chalcogenide microsphere amplifier via particle swarm optimization algorithm

Giuseppe Palma,[a] Pietro Bia,[a] Luciano Mescia,[a] Tetsuji Yano,[b] Virginie Nazabal,[c] Jun Taguchi,[b] Alain Moréac,[d] and Francesco Prudenzano[a,*]
[a]Politecnico di Bari, DEI—Dipartimento di Ingegneria Elettrica e dell'Informazione, Via E. Orabona 4, Bari, 70125, Italy
[b]Tokyo Institute of Technology, Department of Chemistry and Materials, 2-12-1 Ookayama, Meguro-ku Tokyo 15c2-8550, Japan
[c]ISCR, UMR UR1-CNRS 6226, Université de RENNES 1, 35042 RENNES Cedex, France
[d]IPR, UMR CNRS 6626, Université Rennes 1, 35042 Rennes Cedex, France

Abstract. A mid-IR amplifier consisting of a tapered chalcogenide fiber coupled to an Er^{3+}-doped chalcogenide microsphere has been optimized via a particle swarm optimization (PSO) approach. More precisely, a dedicated three-dimensional numerical model, based on the coupled mode theory and solving the rate equations, has been integrated with the PSO procedure. The rate equations have included the main transitions among the erbium energy levels, the amplified spontaneous emission, and the most important secondary transitions pertaining to the ion-ion interactions. The PSO has allowed the optimal choice of the microsphere and fiber radius, taper angle, and fiber-microsphere gap in order to maximize the amplifier gain. The taper angle and the fiber-microsphere gap have been optimized to efficiently inject into the microsphere both the pump and the signal beams and to improve their spatial overlapping with the rare-earth-doped region. The employment of the PSO approach shows different attractive features, especially when many parameters have to be optimized. The numerical results demonstrate the effectiveness of the proposed approach for the design of amplifying systems. The PSO-based optimization approach has allowed the design of a microsphere-based amplifying system more efficient than a similar device designed by using a deterministic optimization method. In fact, the amplifier designed via the PSO exhibits a simulated gain $G = 33.7$ dB, which is higher than the gain $G = 6.9$ dB of the amplifier designed via the deterministic method. [DOI: 10.1117/1.OE.53.7.071805]

Keywords: optics; photonics; light; lasers; chalcogenide glass.

Paper 131663SS received Nov. 4, 2013; revised manuscript received Nov. 27, 2013; accepted for publication Nov. 27, 2013; published online Dec. 23, 2013.

1 Introduction

Optical microresonators are key elements for fabrication of a great variety of photonic devices applied in both linear and nonlinear optics. Generally, the mode resonance is obtained by utilizing two or more mirrors or gratings. Multiple recirculation of light in optical microresonators enables laser oscillation and increases the effective path length, providing a great potential in spectroscopic and interferometric measurements. However, conventional Fabry–Perot resonators have some drawbacks, such as high cost, low compactness, and mechanical instability.[1]

Dielectric spherical microresonators, i.e., dielectric microspheres, allow light confinement in circular orbits by means of repeated total internal reflections occurring at the spherical boundary between the dielectric surface and the surrounding medium. Their surprising properties are related to the resonance of the well-known whispering gallery modes (WGMs), exhibiting high quality factors $Q(10^5 \div 10^9)$ and small mode volumes.

WGMs in fused-silica microspheres have been excited using evanescent field provided by a prism,[2] polished optical fiber coupler,[3,4] and tapered optical fiber.[5] WGM resonances in dielectric microspheres have been investigated and experimented for many applications, e.g., the polarization transmission, coupled-resonator-induced transparency, biosensing, nonlinear optics, quantum electrodynamics, and quantum information processing.[6–8] Moreover, they enable novel functionalities for planar lightwave circuits, such as wavelength selectivity, energy storage and dispersion control, and resonant filtering.[9]

Microspheres doped with rare-earth ions can operate as microcavity amplifiers or lasers. Rare-earth-doped microspheres based on silica, phosphate, tellurite, and ZBLAN (ZrF_4-BaF_2-LaF_3-AlF_3-NaF) glass host materials have been fabricated, obtaining low threshold lasing and very narrow emission linewidth.[8,10–13] As an example, WGMs were excited in Nd^{3+}-doped fluoride glass microsphere by using a $Ti:Al_2O_3$ laser tuned to 800 nm.[14] The laser pump thresholds were found to be 5 and 60 mW for the 1051 and 1334 nm wavelength emissions, respectively.

Chalcogenide glasses exhibit peculiar optical properties, such as a high refractive index, extremely high nonlinearity, photosensitivity, and low phonon energy. WGMs in chalcogenide microspheres have low modal volume. In addition, due to the high refractive index, high absorption and emission cross-sections are measured in these kinds of glasses.[15] However, the low phonon energy induces large radiative decay rates and high quantum efficiency and allows radiative transitions, which are quenched by the multiphonon decay in silica glasses. Moreover, the high rare-earth solubility facilitates the fabrication of efficient lasers and amplifiers.

*Address all correspondence to: Francesco Prudenzano, E-mail: prudenzano@poliba.it

The feasibility of a chalcogenide microsphere has been demonstrated in a variety of works.[15,16–18] As an example, in Ref. 16, the fabrication of chalcogenide microspheres heated by contact with a temperature-controlled ceramic surface has been demonstrated; WGM resonances excited by using tapered silica glass fiber have been observed and a Q factor $>10^5$ was measured close to the wavelength $\lambda = 1.55$ μm. In Ref. 9, with packaged chalcogenide As_2S_3 microspheres using a low refractive index, UV-curable polymer have been fabricated; high-Q modes have been excited at wavelengths close to 1.55 μm in a 110-μm-diameter chalcogenide microsphere via evanescent coupling from a 2-μm-diameter tapered silica fiber.

The need to assemble chalcogenide microsphere via evanescent coupling from tapered silica fiber on feasible planar geometry to be suitably packaged has led the authors to fabricate preliminary microsphere prototypes of chalcogenide glass with the composition of $Ga_5Ge_{20}Sb_{10}S_{65}$ and doped with erbium. Partly truncated spheres, called superspheres, working as a WGM resonator around its equatorial plane, have been lately fabricated via surface-tension mold (StM) technique.[19] The characterization of these prototypes has strongly encouraged the numerical modeling illustrated in this paper.

During the past decades, a large literature has reported experiments on rare-earth-doped microspheres, but only a few papers have addressed simulation models for lasing in microspheres.[20–22] However, accurate numerical modeling is needed for microsphere design and refinement.

In conventional numerical procedures,[20–22] the solution of the rate and power propagation equations is performed by optimizing, one by one, each design parameter. However, the nonlinearity of the equations makes algorithms based on these approaches computationally expensive. Global and stochastic optimization methods are efficient tools to investigate these kinds of problems. As an example, particle swarm optimization (PSO) approaches have been developed for the optimization and characterization of rare-earth-doped photonic crystal fiber amplifiers.[23–25]

In this paper, an amplifying system operating close to 2.7 μm and based on Er^{3+}-doped chalcogenide microsphere coupled to a tapered fiber has been optimized via a PSO approach. An accurate three-dimensional mathematical model for Er^{3+}-doped chalcogenide microspheres[26,27] is employed for calculating the fitness function of the PSO procedure.[23–25] The core of the developed numerical code is based on the coupled mode theory and the rate equations model. In particular, it includes the modal distribution of the optical waves in both tapered fiber and microsphere, and takes into account the most relevant active phenomena in Er^{3+}-doped chalcogenide glasses, such as the absorption rates at both pump and signal wavelengths, the stimulated emission rate at signal wavelength, the amplified spontaneous emission noise, the lifetime and branching ratios of the considered energy levels, the ion-ion energy transfers, and the excited state absorption. The design is realistically performed on the basis of the optical and spectroscopic parameters measured on chalcogenide glass[26–28] and by considering the coupling of the microsphere with a tapered fiber.

The PSO approach has given good results, allowing a global optimization of the microsphere amplifier by varying simultaneously a number of design parameters. As a result, an improvement of the simulated gain of the microsphere amplifier from $G = 6.9$ dB, found with the deterministic approach (DA)[26] for a very similar device, to $G = 33.7$ dB found in this paper with PSO, has been obtained. The numerical results underline that due to the high number of design parameters to be optimized, a deterministic solution searching strategy does not allow an efficient design in these kinds of problems.

2 Theory

The amplifying system consists of a tapered optical fiber placed close to the equator of an Er^{3+}-doped chalcogenide microsphere. Figure 1 illustrates a sketch of the amplifying system. A detailed description of the model (without PSO) is reported by the authors in Ref. 26.

The azimuthal, polar, and radial distributions of WGMs are given by the complex exponential functions, Hermite polynomials, and spherical Bessel functions, respectively. Each WGM can be identified by three integers n, l, and m. WGMs with higher spatial overlap with the fiber taper have their power bounded near the equatorial plane ($m = l$ and $n = 1$). The coupling of the optical power between the tapered fiber and the undoped microsphere is modeled by using the coupled mode theory.[29–31] The time domain evolution of the amplitude A of the internal cavity electromagnetic field at the pump p and the signal s wavelength can be obtained by solving the following differential equations:[26,30–35]

$$\begin{aligned}\frac{dA^p_{l,m,n}}{dt} &= -\frac{1}{2}\left(\frac{1}{\tau_{ext}} + \frac{1}{\tau_0} - g^p_{l,m,n} - 2i\Delta\omega\right)A^p_{l,m,n} \\ &\quad + i\sqrt{\frac{1}{\tau_{ext}\tau}}A^p_{in,l,m,n} \\ \frac{dA^s_{l,m,n}}{dt} &= -\frac{1}{2}\left(\frac{1}{\tau_{ext}} + \frac{1}{\tau_0} - g^s_{l,m,n} - 2i\Delta\omega\right)A^s_{l,m,n} \\ &\quad + \frac{c}{2n_{eff}}\sum_q N^q_j\sigma_{ji}(\tilde{\nu})\Gamma^{q,s}_{l,m,n}A_0 + i\sqrt{\frac{1}{\tau_{ext}\tau}}A^s_{in,l,m,n},\end{aligned} \tag{1}$$

with

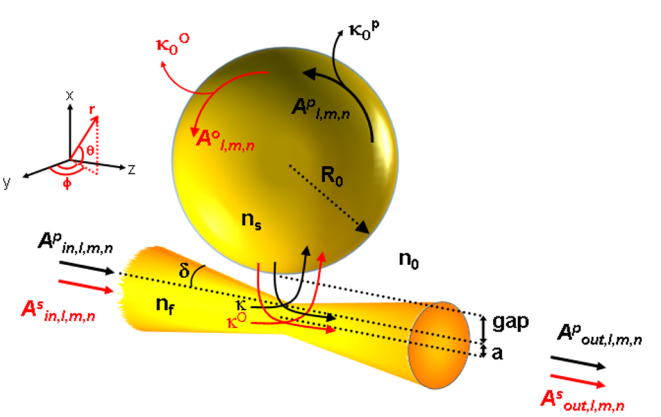

Fig. 1 Layout sketch of the chalcogenide fiber taper coupled to the Er^{3+}-doped chalcogenide microsphere.

$$g^a_{l,m,n} = \frac{c}{n_{\text{eff}}}\left[\sum_q N^q_j \sigma_{ji}(\tilde{\nu})\Gamma^{q,a}_{l,m,n} - \sum_q N^q_i \sigma_{ij}(\tilde{\nu})\Gamma^{q,a}_{l,m,n}\right] \quad (2)$$

with $a = p, s$.

The gain G for the amplifier is related to the objective function to be maximized via PSO.

$$G = \left|\frac{A^a_{\text{out},l,m,n}}{A^a_{\text{in},l,m,n}}\right|^2 = \left|\sqrt{1-\frac{\tau}{\tau_{\text{ext}}}} + i\sqrt{\frac{\tau}{\tau_{ext}}}\frac{A^a_{l,m,n}}{A^a_{\text{in},l,m,n}}\right| \quad (3)$$

with $a = p, s$.

$A_{\text{in},l,m,n}$ and $A_{\text{out},l,m,n}$ are the amplitudes of mode electric field at the input and at the output fiber section and coupled with the l,m, n WGM mode of the microsphere; $\tau = 2\pi R_0 n_{\text{eff}}/c$ is the circulation time inside the microsphere, n_{eff} is the WGM effective refractive index, c is the speed of light in vacuum; $\Delta\omega = \omega_{\text{in}} - \omega_{\text{WGM}}$ is the frequency detuning of the fiber input signal from the WGM resonance frequency; $\tau_0 = 1/\kappa_0^2 = Q_0/\omega_{\text{WGM}}$ is the coupling lifetime, where Q_0 is the intrinsic quality factor and κ_0 is the intrinsic cavity decay rate; $\tau_{\text{ext}} = m\pi/(\omega\kappa^2)$ is the coupling lifetime, κ is the cavity decay rate or coupling coefficient; $\tilde{\nu} = \nu_{l,m,n}$ is the WGM resonant frequency; $\sigma_{i,j}(\tilde{\nu})$ is the erbium cross-section at frequency $\tilde{\nu}$; $A^a_{l,m,n}$ is the slowly varying amplitude scaling the normalized electric field $E^a_{l,m,n}$ on the $r-\theta$ plane; $\Gamma^{q,a}_{l,m,n}$ with $a = p, s$ is the overlap factor of each WGM with the rare-earth profile in the q'th sector (the microsphere doped area is divided in q sector in the $r-\theta$ plane); and N^q_i $i = 1, 2, \ldots 6$ is the ion population concentration of i'th energy level in the q'th sector.[26]

Design and optimization of rare-earth-doped glass amplifiers are typically based on the deterministic optimization methods. The optimal amplifier length, the rare-earth concentration, the waveguide transversal section, and all the other design parameters are identified one at a time. The up-conversion and cross-relaxation phenomena induce nonlinearities in rare-earth-doped glass amplifier model. As a result, the optimization problem is difficult to be performed, especially in a rare-earth-doped microsphere amplifier, where a number of geometrical parameters have to be finely optimized. Moreover, deterministic algorithms can exhibit stagnation problems in local maxima/minima during the global optimization search of the objective functions (e.g., gain, bandwidth, output power, signal-to-noise ratio). The stochastic nature of the PSO algorithm allows a high efficiency in optimization of a large number of parameters for its ability to avoid local maxima/minima and operate in discontinuous solution domains.

The PSO algorithm is inspired by the behavior of a swarm (populations) of M individuals of bees (trial solutions or particles), which fly in a field (N-dimensional search space) to search for food, i.e., high density of flowers (to maximize/minimize a fitness function). A flow chart of the PSO algorithm is illustrated in Fig. 2. Each particle p_i is characterized by a position x_i constituting a trial solution. The trial solution goodness is evaluated by means of the fitness function.[36,37] The bee positions (solutions) are updated by applying the operator v_i, called velocity, which is dynamically adjusted according to the historical behaviors of the particle fly in order to maximize/minimize the suitable fitness function. At first, each bee (particle) has a random position and a random velocity; then its trajectory is modified by keeping track of its location in the solution space and by taking into account both the previous location giving the best fitness value experimented by the single particle (personal best, P_{best}) and highest fitness location discovered by the entire swarm (global best, G_{best}). In this way, the entire swarm moves toward positions characterized by maximized/minimized values of a fitness function.

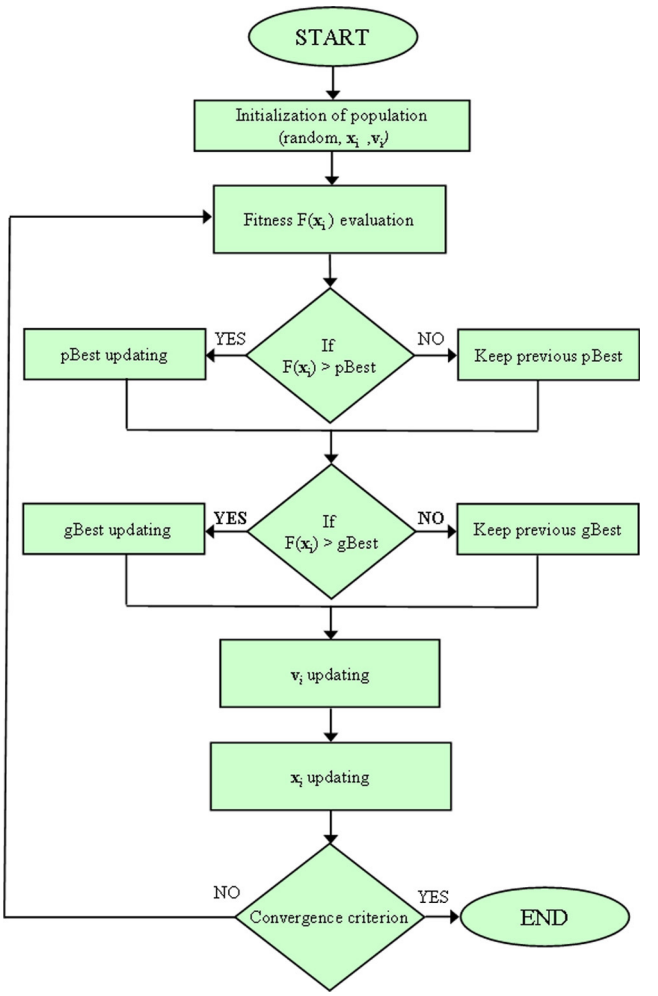

Fig. 2 Flow chart of the particle swarm optimization (PSO) algorithm.

More precisely, the position $\mathbf{x}_i$ and the velocity $\mathbf{v}_i$ vectors of the particles at each iteration are updated by means of the following set of equations:[36,37]

$$\boldsymbol{v_i}(n+1) = w \times \boldsymbol{v_i}(n) + c_1 \times r_1 \times [\boldsymbol{x_{bi}}(n) - \boldsymbol{x_i}(n)] + c_2 \times r_2 \times [\boldsymbol{x_g}(n) - \boldsymbol{x_i}(t)], \quad (4)$$

$$\boldsymbol{x_i}(n+1) = \boldsymbol{x_i}(n) + \boldsymbol{v_i}(n+1), \quad (5)$$

where $\mathbf{x}_{bi}(n)$ is the best previous position of the i'th particle, $\mathbf{x}_g(n)$ is the best position among all the particles in the population, w is the inertia weight, c_1 and c_2 are positive constants, called cognitive and social parameters, and r_1 and r_2 are positive numbers randomly generated between 0 and 1 to inject a stochastic behavior in the searching procedure.[23–25]

3 Design and Synthesis of $Er^{3+}:Ga_5Ge_{20}Sb_{10}S_{65}$ Chalcogenide Microsphere Amplifier

In this section, PSO numerical modeling, aimed to identify the optimal fiber taper coupled $Er^{3+}:Ga_5Ge_{20}Sb_{10}S_{65}$ chalcogenide microsphere amplifier, operating in the mid-IR wavelength range is illustrated. The motivation is related to the good experimental results obtained by applying StM technique to fabricate the aforesaid erbium-doped chalcogenide glass microsphere.[19] The bulk glass sample was prepared by a conventional melting and quenching method in a silica glass ampoule.[38] The fabricated glass was crushed into a powder of <200 μm. The crushed glass powders were classified using sieves in the range of 20 to 40 μm and 40 to 80 μm, washed by iso-propanol under ultrasonic wave, and finally, dried in air for a day. These powders were put on a polished glassy carbon substrate and heated at 515°C for 5 min on the electric furnace settled in a glove box filled with dry Ar gas or in a furnace with a flux of Ar and H_2S gas.

As shown in Fig. 3, the StM technique realizes the formation of a superspherical shape because the contact angle of 2S2G glass is $\theta > 90$ deg, as a glassy carbon is a favorable substrate to induce low wettability of the molten chalcogenide glass. Quitea high Q factor can be realized in a truly spherical particle made of the extremely transparent material without scattering inclusion and contaminant on and/or inside the sphere. Therefore, when we desire the preparation of a superspherical optical resonator of $Ga_5Ge_{20}Sb_{10}S_{65}$ glass by the StM technique, we have to pay attention to the factors of shape (curvature of sphere) and the surface scattering. The percentage of prepared superspheres with high sphericity and/or circularity at the equatorial plane was ~10%, and their deviation to circularity was <3%. These values are good enough to use them for an optical resonator. The glass transition temperature of $Ga_5Ge_{20}Sb_{10}S_{65}$ glass is sensitive to the atomic ratio of sulfur to the metals. Lower sulfur content increases the glass transition temperature and could decrease the thermal stability of glass against crystallization. The precipitation of crystal is energetically easy on the heterogeneous interface like glass surface. A Raman spectroscopy investigation of the sulfide glass supersphere was done and the above hypothesis was confirmed. Once α-GeS_2 crystallites appear on the surface of the molten glass droplet, it corrupts the balance of the surface tension in the particle and produces a distorted supersphere. In order to make a good spherical surface and improve its Q factor, the surface crystallization has to be suppressed well. Therefore, strict control of sulfur content of the $Ga_5Ge_{20}Sb_{10}S_{65}$ glass is requisite for the preparation of optical resonator made of glass by the StM technique. The results were significantly improved when a mixture of H_2S/Ar gas was employed during the StM heat treatment; this is an essential way of reducing the crystal surface formation. Thanks to the optimized StM process enabling superspherical microsphere fabrication in the diameter range of 5 to 50 μm, WGMs were observed for these microspheres concerning their luminescence around 650 nm using the Raman spectrophotometer, and a luminescence centered at ~2775 nm corresponding to the ${}^4I_{11/2} \rightarrow {}^4I_{13/2}$ transition was also experimentally observed from $Er^{3+}:Ga_5Ge_{20}Sb_{10}S_{65}$ glass pumped at 980 nm (Fig. 4). These experimental observations augur well to obtain lasing demonstration in microspheres made of $Er^{3+}:Ga_5Ge_{20}Sb_{10}S_{65}$ and have encouraged us to develop the PSO modeling to consider an effective evanescent wave coupling of the $Er^{3+}:Ga_5Ge_{20}Sb_{10}S_{65}$ microsphere, allowing laser emission in the mid-IR spectral range.

In the PSO modeling, the pump wavelength is close to $\lambda_p = 980$ nm and the signal wavelength is close to $\lambda_s = 2770$ nm. The size of the fiber taper has to be designed to ensure the fundamental mode propagation and a suitable evanescent field in the fiber-microsphere gap. In order to carry out a realistic optimization and, therefore, an actual evaluation of the device feasibility, the simulations have been performed by taking into account the refractive index wavelength dispersion by means of the Sellmeier equation [26,28] and the measured spectroscopic parameter summarized in Table 1.[28]

The absorption and emission cross-sections affect the competition among a number of different resonant WGMs. As an example, the absorption cross-section at the pump wavelength $\lambda = 986$ nm is close to 1.32×10^{-24} m^2, while the emission cross-section at the signal wavelength $\lambda = 2770$ nm is close to 1.4×10^{-24} m^2. Different emission and absorption cross-section values are considered for the different WGM resonance frequencies. The thickness of the erbium-doped region (near the microsphere surface) and the erbium concentration are $s = 3$ μm and $N_{Er} = 0.5$ w%,

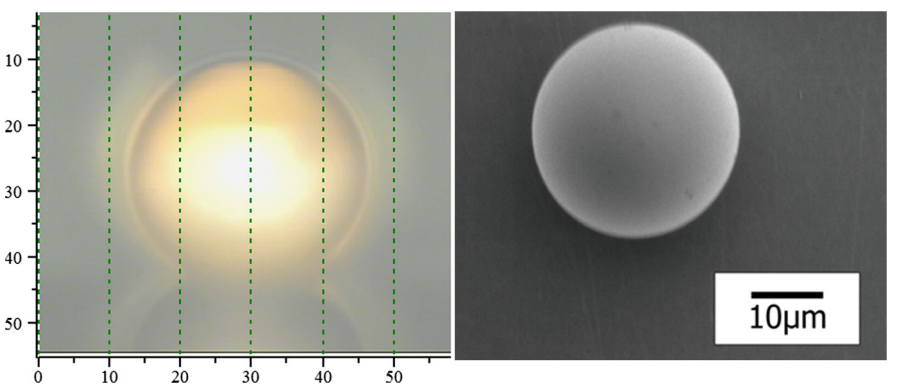

Fig. 3 Optical microscope and SEM image of $Er^{3+}:Ga_5Ge_{20}Sb_{10}S_{65}$ micrometer microsphere coated with Au/Pd conductive layer at the surface for SEM imaging.

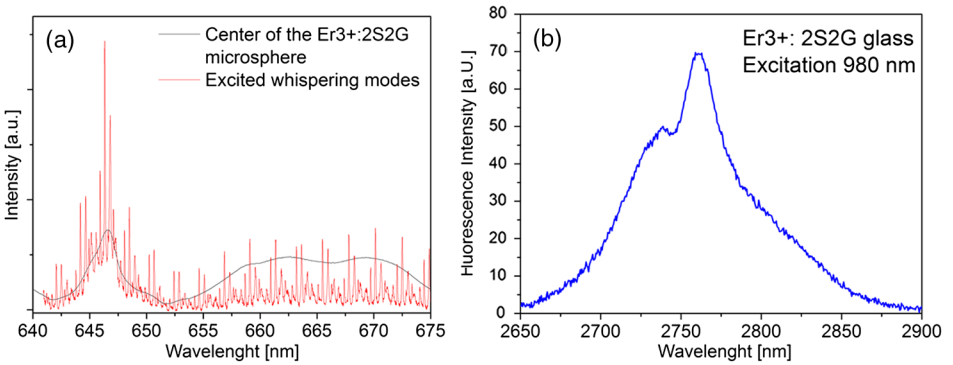

Fig. 4 Feasibilty investigation: (a) Raman and fluorescence spectra for 633 nm excitation in the center and border of an equatorial plane of the $Er^{3+}:Ga_5Ge_{20}Sb_{10}S_{65}$ microsphere. (b) Fluorescence spectrum of $Er^{3+}:Ga_5Ge_{20}Sb_{10}S_{65}$ glass excited at 980 nm.

Table 1 Spectroscopic parameters of the Er^{3+}-doped chalcogenide glass.[27]

Energy level transitions	Wavelength (nm)	Lifetime (ms)	Branching ratio (%)
$^4I_{13/2} \rightarrow {}^4I_{15/2}$	1531.7	$\tau_2 = 1.83$	$\beta_{21} = 100$
$^4I_{11/2} \rightarrow {}^4I_{15/2}$	986.4	$\tau_3 = 1.37$	$\beta_{31} = 86.28$
$^4I_{11/2} \rightarrow {}^4I_{13/2}$	2770.7	$\tau_3 = 1.37$	$\beta_{32} = 13.72$
$^4I_{9/2} \rightarrow {}^4I_{15/2}$	810.0	$\tau_4 = 1.08$	$\beta_{41} = 80.38$
$^4I_{9/2} \rightarrow {}^4I_{13/2}$	1719.1	$\tau_4 = 1.08$	$\beta_{42} = 18.82$
$^4I_{9/2} \rightarrow {}^4I_{11/2}$	4529.4	$\tau_4 = 1.08$	$\beta_{43} = 0.80$
$^4F_{9/2} \rightarrow {}^4I_{15/2}$	662.7	$\tau_5 = 0.13$	$\beta_{51} = 91.99$
$^4F_{9/2} \rightarrow {}^4I_{13/2}$	1168.1	$\tau_5 = 0.13$	$\beta_{52} = 4.32$
$^4F_{9/2} \rightarrow {}^4I_{11/2}$	2019.4	$\tau_5 = 0.13$	$\beta_{53} = 3.34$
$^4F_{9/2} \rightarrow {}^4I_{9/2}$	3623.1	$\tau_5 = 0.13$	$\beta_{54} = 0.35$

respectively. The input pump power is $P_p = 100$ mW and the input signal power $P_s = -50$ dBm.

The approach based on swarm intelligence is employed in the design to obtain values of parameters maximizing the optical gain. In particular, the PSO is applied to optimize microsphere radius R_0, taper waist radius a, taper angle δ, and taper-microsphere gap g. Therefore, the algorithm described in Sec. 2 is written by defining a swarm composed of $N = 32$ particles. The position vector of the i'th particle is $\mathbf{x}_i = [R_o^i, a^i, \delta^i, g^i]^T$, with $i = 1, 2, \ldots, \mathrm{N}$. The fitness function is:

$$F(\mathbf{x}_i) = 10 \log \mathrm{G}(\mathbf{x}_i).$$

The PSO parameters have been tuned heuristically by evaluating the solution space characteristic. On the basis of previous working experiences, the limits of the considered parameters have been roughly fixed such that the maximum gain is expected to lie in suitable ranges. The parameters used in PSO algorithm and the solution space limits are summarized in Table 2.

Table 2 Parameters and solution space limits used in particle swarm optimization (PSO) algorithm.

Variable	Value
Social parameter	1.494
Cognitive parameter	1.494
Inertia weight	Linearly spaced vector from 0.9 to 0.4
Iteration limit	32
Number of particles	32
$[p_{\min}, p_{\max}]$ for R_o (μm)	10 ÷ 50
$[p_{\min}, p_{\max}]$ for a (nm)	500 ÷ 800
$[p_{\min}, p_{\max}]$ for δ (rad)	0.001 ÷ 0.04
$[p_{\min}, p_{\max}]$ for g (nm)	500 ÷ 1000

The PSO simulations have been performed by considering many WGMs in the wavelength band from 2740 to 2820 nm. The PSO has allowed the identification of the maximum gain (global best) for the $\mathrm{WGM}_{1,217,217}$ with the following optimal parameters: microsphere radius $R_0 = 45$ μm, taper waist radius $a = 517$ nm, taper angle $\delta = 0.03$ rad, and taper-microsphere gap $g = 512$ nm. By simulations, slight variations (tens of nanometers) of taper waist radius and taper-microsphere gap induce low gain changes (~1 dB). By varying the parameter n from 1 to 3, 18 different resonant WGMs were simulated. The parameters n, l, and m, the WGM resonance wavelengths, the output powers, and the optical gains are reported in Table 3.

For each WGM, the proper resonance frequency is taken into account in order to evaluate all the spectroscopic and physical parameters (refractive index, emission cross-section, absorption cross-section, etc.) affecting the competition with the other WGMs. The modes with $n = 1, 2, 3$ and $m = l$ have been considered in the simulation. WGMs with different values of l and m have not been considered because they exhibited a low overlapping factor $\Gamma_{l,m,n}^{q,s}$. Table 4 reports the comparison among the parameter values calculated by the proposed PSO algorithm and those obtained with the

Table 3 PSO optimized amplifier. Parameters $l = m$ and n of whispering gallery mode, resonance wavelength, output power, and optical gain.

$l = m$ values	n values	WGM resonance wavelength (nm)	P_{out} (dBm)	Optical gain G (dB)
213	1	2813.4	−37.2778	12.7222
214	1	2801.7	−35.1063	14.8937
215	1	2788.0	−33.5839	16.4161
216	1	2776.5	−27.0753	22.9247
217	1	2763.1	−16.2846	33.7154
218	1	2750.8	−33.5089	16.4911
205	2	2808.4	−46.8126	3.1874
206	2	2795.5	−46.4806	3.5194
207	2	2782.8	−46.1096	3.8904
208	2	2770.1	−45.2190	4.7810
209	2	2757.7	−45.4078	4.5922
210	2	2745.5	−46.6880	3.3120
198	3	2810.3	−49.0198	0.9802
199	3	2797.3	−48.9377	1.0623
200	3	2784.4	−48.8623	1.1377
201	3	2771.7	−48.6747	1.3253
202	3	2759.1	−48.6556	1.3444
203	3	2746.6	−48.9811	1.0189

deterministic DA one illustrated in Ref. 26. The use of a deterministic method requires a suitable discretization for R_0, a, δ, g and thus the investigation of an extremely high number of different cases with a very large time consumption.

Table 5 reports the characteristics of the PSO optimized amplifier. A low intrinsic signal lifetime τ_0, resulting in low losses, is calculated. The results reported in Tables 3 to 5 show that the proposed PSO approach finds solutions more efficiently than the deterministic one.[26]

Table 4 Comparison between deterministic approach (DA) and PSO: gain, microsphere radius R_o, taper waist radius a, taper angle δ, and taper-microsphere gap.

Variable	DA value	PSO value
DA maximum gain/fitness global best (dB)	6.9	33.7
Microsphere radius (μm)	25	45
Taper waist radius (nm)	700	517
Taper angle (rad)	0.03	0.02
Taper-microsphere gap (nm)	560	512

Table 5 Characteristics of the PSO optimized amplifier.

Variable	Value
Signal WGMs mode	$n = 1$, $l = m = 217$
Signal wavelength λ_s (nm)	2763.1
Signal refractive index of microsphere n_s and taper n_f	2.2253
Pump WGMs mode	$n = 1$, $l = m = 641$
Pump wavelength λ_p (nm)	979.9
Intrinsic signal lifetime τ_0 (μs)	0.1357
Coupling signal lifetime τ_{ext} (ns)	0.2248
Optical gain (dB)	33.7

A high number of PSO launches have been performed. In almost all cases, ~18 iterations were required for convergence, obtaining a global best close to 33.7 dB.

The discrepancy in the calculated maximum gain observed between the DA, $G = 6.9$ dB, and the PSO, $G = 33.7$ dB, is due to the higher efficiency of global optimization approach, allowing a better design to parity of calculation time consumption. In fact, PSO can optimize simultaneously a high number of parameters through an automated global solution search. On the contrary, in DA, to avoid an extremely large time consumption, a parameter at a time is varied, by fixing all the others which are supposed to be optimized (local search). A global search could be performed with a DA, but a very high number of simulation cases are required. The DA simulation number is related to the calculation accuracy (parameter quantization/discretization) and to the number of parameters to be optimized. When the designer chooses the most promising DA simulation cases, some particular configurations can be neglected, thus losing the best configuration. Therefore, in this paper, PSO has allowed the identification of a specific amplifier configuration not included in the deterministic investigation illustrated in Ref. 26.

The performance of the PSO approach can be easily understood by the example of Fig. 5. It illustrates the PSO solution: (a) microsphere radius R_0 and taper waist radius a; (b) taper angle δ and taper-microsphere gap g. The color represents the optical gain corresponding to each particle. It is worthwhile to note that many particles are located in a small region around the maximum gain value (global best).

Figure 6 illustrates the fitness $F(\mathbf{x}_i)$ corresponding to the global best (i.e., gain G in decibel, calculated for the global best of the swarm) versus iteration number. The best particle provides a gain very close to the maximum one after only 18 iterations. This confirms that the algorithm enables one to find solutions quickly.

The simulation results indicate that the proposed Er^{3+}-doped chalcogenide microsphere amplifier, evanescently coupled with a tapered optical fiber, seems very promising and could find interesting applications. Although good $Ga_5Ge_{20}Sb_{10}S_{65}$ have been fabricated and characterized, the amplifier construction is related to the nontrivial problem

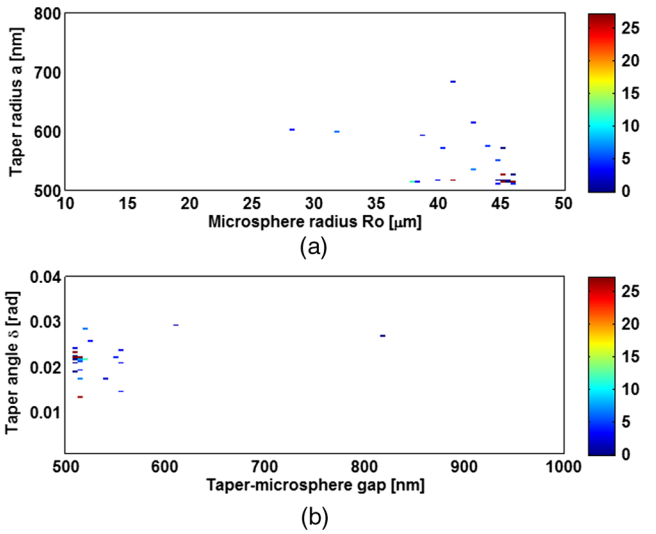

Fig. 5 PSO optimized solutions: (a) Microsphere radius R_0 and fiber taper radius a. (b) Gap g and taper angle δ.

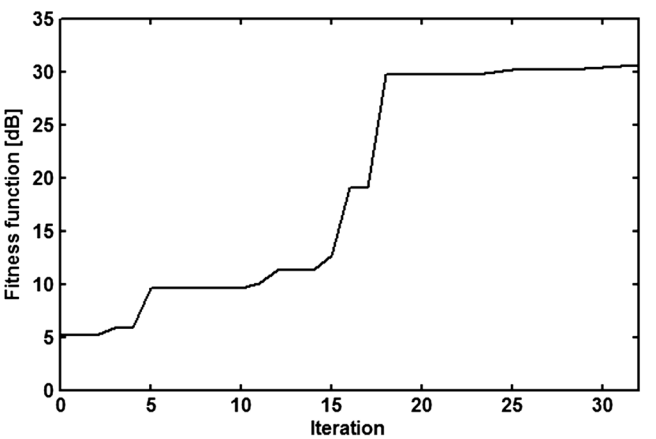

Fig. 6 Fitness function corresponding to global best versus iterations.

of drawing a suitable $Ga_5Ge_{20}Sb_{10}S_{65}$ fiber taper with very small radius. Therefore, further technological efforts will be dedicated in future to this aim. For instance, an integrated optical system can be envisaged to overcome the fragility of fiber taper for such dimensions.[39]

4 Conclusions

In this paper, an accurate design of Er^{3+}-doped chalcogenide microsphere amplifier evanescently coupled with a tapered optical fiber has been performed. The amplifying system has been optimized via a PSO procedure for operation close to 2770 nm. The PSO has provided surprising performance in terms of convergence and efficiency, allowing a global optimization of the microsphere amplifier. An improvement of the simulated gain of the microsphere amplifier from $G = 6.9$ dB, found using DA, to $G = 33.7$ dB, found in this paper using PSO, has been obtained. This demonstrates that a deterministic solution searching strategy does not allow an efficient design in these kinds of problems. Moreover, the simulation results indicate that the proposed Er^{3+}-doped chalcogenide microsphere amplifier, evanescently coupled with a tapered optical fiber, is feasible after drawing a suitable $Ga_5Ge_{20}Sb_{10}S_{65}$ fiber taper with radius close to 517 nm.

References

1. A. B. Matsko and V. S. Ilchenko, "Optical resonators with whispering-gallery modes—Part I: Basics," *IEEE J. Sel. Topics Quantum Electron.* **12**(1), 3–13 (2006).
2. M. L. Gorodetsky and V. V. Ilchenko, "High-Q optical whispering gallery microresonators: precession approach for spherical mode analysis and emission patterns with prism couplers," *Opt. Commun.* **113**(1–3), 133–143 (1994).
3. A. Serpenguzel, S. Arnold, and G. Griffel, "Excitation of resonances of microspheres on an optical fiber," *Opt. Lett.* **20**(7), 654–656 (1995).
4. F. Treussart et al., "Microlasers based on silica microspheres," *Ann. Telecommun.* **52**(11–12), 557–568 (1997).
5. J. C. Knight et al., "Phase-matched excitation of whispering gallery mode resonances using a fiber taper," *Opt. Lett.* **22**(15), 1129–1131 (1997).
6. H.-C. Ren et al., "High-Q microsphere biosensor-analysis for adsorption of rodlike bacteria," *Opt. Express* **15**(25), 17410–17423 (2007).
7. F. Vollomer and A. Stephen, "Whispering-gallery-mode biosensing: label-free detection down to single molecules," *Nature Methods* **5**(7), 591–596 (2008).
8. L. Yang and K. J. Vahala, "Gain functionalization of silica microresonators," *Opt. Lett.* **28**(8), 592–594 (2003).
9. P. Wang et al., "Packaged chalcogenide microsphere resonator with high Q-factor," *Appl. Phys. Lett.* **102**(13), 131110 (2013).
10. G. S. Murugan et al., "Integrated Nd-doped borosilicate glass microsphere laser," *Opt. Lett.* **36**(1), 73–75 (2011).
11. S.Y. Chen et al., "Characteristics of Er and Er-Yb-Cr doped phosphate microsphere fibre lasers," *Opt. Commun.* **282**(18), 3765–3769 (2009).
12. P. Feron, "Whispering gallery mode lasers in erbium doped fluoride glasses," *Annales de la Fondation Louis de Broglie* **29**(1–2), 317–329 (2004).
13. G. N. Conti et al., "Spectroscopic and lasing properties of Er^{3+} doped glass microspheres," *Non Cryst. Solids* **352**(23–25), 2360–2363 (2006).
14. K. Miura, K. Tanaka, and K. Hirao, "CW laser oscillation on both the 4F3/2 – 4I11/2 and 4F3/2 – 4I13/2 transitions of Nd3+ ions using a fluoride glass microsphere," *J. Non Cryst. Solids* **213–214**, 276–280 (1997).
15. G. R. Elliot et al., "Chalcogenide glass microspheres; their production, characterization and potential," *Opt. Express* **15**(26), 17542–17553 (2007).
16. P. Wang et al., "Chalcogenide microsphere fabricated from fiber tapers using contact with a high-temperature ceramic surface," *IEEE Photon. Technol. Lett.* **24**(13), 1103–1105 (2012).
17. C. Grillet et al., "Fiber taper coupling to chalcogenide microsphere modes," *Appl. Phys. Lett.* **92**(17), 171109–171111 (2008).
18. D. H. Broaddus et al., "Silicon-waveguide-coupled high-Q chalcogenide microspheres," *Opt. Express* **17**(8), 5998–6003 (2009).
19. T. Yano, S. Shibata, and T. Kishi, "Fabrication of micrometer-size glass solid immersion lens," *J. Appl. Phys. B* **83**(2), 167–170 (2006).
20. L. Mescia et al., "Design of rare-Earth-doped microspheres," *IEEE Photon. Techonol. Lett.* **22**(6), 422–424 (2010).
21. T. Kouki and T. Makoto, "Optical microsphere amplification system," *Opt. Lett.* **32**(21), 3197–3199 (2007).
22. Y.G. Boucher and P. Féron, "Generalized transfer function: a simple model applied to active single-mode microring resonators," *Opt. Commun.* **282**(19), 3940–3947 (2009).
23. A. Giaquinto et al., "Particle swarm optimization-based approach for accurate evaluation of upconversion parameters in Er^{3+}-doped fibers," *Opt. Lett.* **36**(2), 142–144 (2011).
24. L. Mescia et al., "Particle swarm optimization for the design and characterization of silica-based photonic crystal fiber amplifiers," *J. Non Cryst. Solids* **357**(8–9), 1851–1855 (2011).
25. S. Girard et al., "Design of radiation-hardened rare-Earth doped amplifiers through a coupled experiment/simulation approach," *J. Lightwave Technol.* **31**(8), 1247–1254 (2013).
26. L. Mescia et al., "Design of mid-infrared amplifiers based on fiber taper coupling to erbium-doped microspherical resonator," *Opt. Express* **20**(7), 7616–7629 (2012).
27. L. Mescia et al., "Design of mid-IR Er^{3+}-doped microsphere laser," *IEEE Photon. J.* **5**(4), 1501308 (2013).
28. F. Prudenzano et al., "Theoretical study of cascade laser in erbium-doped chalcogenide glass fibers," *Opt. Mater.* **33**(2), 241–245 (2010).
29. B. E. Little, J.-P. Laine, and H. A. Haus, "Analytic theory of coupling from tapered fibers and half-blocks into microsphere resonators," *J. Lightwave Technol.* **17**(4), 704–715 (1999).
30. M. L. Gorodetsky and V. S. Ilchenko, "Optical microsphere resonators: optimal coupling to high-Q whispering-gallery modes," *J. Opt. Soc. Am. B* **16**(1), 147–154 (1999).

31. C.-L. Zou et al., "Taper-microsphere coupling with numerical calculation of coupled-mode theory," *J. Opt. Soc. Am. B* **25**(11), 1895–1898 (2008).
32. H. A. Haus, *Waves and Fields in Optoelectronics*, Prentice Hall Inc., New Jersey (1984).
33. M. J. F. Digonnet, *Rare-Earth-Doper Fider Lasers and Amplifiers*, Marcel Dekker Inc., New York (2001).
34. K. Vahala, *Optical Microcavitie*, World Scientific Publishing, Singapore (2004).
35. A.W. Snyder and J. D. Love, *Optical Waveguide Theory*, Chapman and Hall, London (1988).
36. J. Robinson and Y. Rahmat-Samii, "Particle swarm optimization in electromagnetics," *IEEE Trans. Antennas Propag.* **52**(2), 397–407 (2004).
37. N. Jin and Y. Rahmat-Samii, "Advances in particle swarm optimization for antenna designs: real-number, binary, single-objective and multi-objective implementations," *IEEE Trans. Antennas Propag.* **55**(3), 556–567 (2007).
38. V. Moizan et al., "Er^{3+}-doped GeGaSbS glasses for mid-IR fibre laser application: synthesis and rare earth spectroscopy," *Opt. Mater.* **31**(1), 39–46 (2008).
39. J. Charrier et al., "Sulphide GaxGe25-xSb10S65 ($x = 0, 5$) sputtered films: elaboration and optical characterisation of planar and rib optical waveguides," *J. Appl. Phys.* **104**(7), 073110 (2008).

Giuseppe Palma received the degree in electronic engineering from the Politecnico di Bari in September 2013. He has received a scholarship for postgraduate research activity at the Dipartimento di Ingegneria Elettrica e dell'Informazione of the Politecnico di Bari. His research activity regards the modeling of active microspheres and substrate integrated waveguides. He is a member of the Italian Society of Optics and Photonics (SIOF).

Pietro Bia received bachelor's and master's degrees in 2008 and 2010, respectively. During 2011 he received a scholarship for postgraduate research activities for the topic: "Design of innovative cladding-pumped fiber lasers, nonlinear effects induced by high optical power density and microsphere laser." Since 2012 he has been a PhD student of Politecnico di Bari. He is a member of Italian Society of Optics and Photonics (SIOF-EOS) and Italian Society of Electromagnetism (SIEm).

Luciano Mescia received his PhD degree in electromagnetic fields in 2003. His research interests include the development of artificial neural networks, genetic algorithm, swarm intelligence applied to rare earth doped fiber lasers and amplifiers. He is performing studies regarding the design of innovative antenna array for energy harvesting applications, the analysis and synthesis of novel dielectric lens antennas operating in the microwave and millimeter frequency range, the development of novel FDTD schemes based on fractional calculus.

Tetsuji Yano is an associate professor at Tokyo Institute of Technology. He received his BS, MS, and doctor of engineering from Tokyo Institute of technology. His current research covers the glass materials processing and their application including optical functionalities of devices of glass.

Virginie Nazabal graduated from the Paris VI University and the Bordeaux University for PhD, in 1999. She joined the NIMS (Japan) for JSPS fellowship position for two years and the CNRS since 2001 (Glass & Ceramic team, ISCR, Rennes University). Her research interests concern vitreous materials for optics with nearly 100 publications. She received in 2010 a bronze medal of CNRS and a Pollutec-Ademe award in 2011 for innovative techniques for the environment.

Jun Taguchi was a PhD candidate at Tokyo Institute of Technology at the time when this research was in progress. He received BS, MS, and doctor of engineering from Tokyo Institute of Technology. At the present, he is a researcher at Corning Incorporated, Japan.

Alain Moréac received the PhD degree in physics (University Rennes 1—France) in 1995. In 1996, he joined DILOR (Lille, France), which became Jobin-Yvon Raman Division (today Horiba Scientific (Villeneuve d'Ascq, France): he was manager of the Raman Service & Quality Control Team. Since 2003, he belongs to the Institute of Physics of Rennes (University Rennes 1) as engineer for research. He is in charge of Raman spectroscopy, extended to the university's Raman platform.

Francesco Prudenzano graduated in electronic engineering from the University of Bari in April 1990. Since 2003 he has been associate professor in electromagnetic fields at Politecnico di Bari. His research activity includes modeling and characterization of optical and microwave devices, substrate integrated waveguides, rare earth doped photonic crystal fibers, optical sensors, and nonlinear optics. He has co-authored over 320 publications, 240 published in journals and international conferences. He is involved in several national and international research projects and co-operations.